27TH EUROPEAN ROTORCRAFT FORUM

Session Aerodynamics
Paper #38

AERODYNAMICS OF HELICOPTER. APPLICATION OF THE NAVIER-STOKES CODES DEVELOPED IN THE FRAMEWORK OF THE JOINED GERMAN/FRENCH CFD RESEARCH PROGRAM CHANCE

by

A. D'Alascio
Eurocopter Deutschland GmbH, 81663 München, Germany

K. Pahlke
DLR, Deutsche Forschungsanstalt für Luft und Raumfahrt e.V. Braunschweig, Germany

C. Castellin
Eurocopter, Marignane, France

M. Costes
ONERA, Office National d'Études et de Recherches Aérospatiales, Chatillon, France

SEPTEMBER 11 - 14, 2001
MOSCOW
RUSSIA

AERODYNAMICS OF HELICOPTER. APPLICATION OF THE NAVIER-STOKES CODES DEVELOPED IN THE FRAMEWORK OF THE JOINED GERMAN/FRENCH CFD RESEARCH PROGRAM CHANCE

A. D'Alascio
Eurocopter Deutschland GmbH, 81663 München, Germany

K. Pahlke
DLR, Deutsche Forschungsanstalt für Luft und Raumfahrt e.V. Braunschweig, Germany

C. Castellin
Eurocopter, Marignane, France

M. Costes
ONERA, Office National d'Études et de Recherches Aérospatiales, Chatillon, France

In research centres and universities, both in the US and Europe, considerable effort is being put into the development and validation of advanced CFD methods based on the solution of the Navier-Stokes equations. Within the frame of the French-German project CHANCE (supported by the French DPAC and the German BMWi), the research institutes ONERA and DLR are enhancing the CHANCE CFD flow solvers (FLOWer and elsA), together with the helicopter manufacturer Eurocopter (in Marignane, France and Ottobrunn, Germany) that is validating them against test cases of industrial interest. These CFD codes are also being integrated in rotor and fuselage design systems at Eurocopter [1]. The validation activity of the flow solvers will be achieved through intermediate stages of increasing geometry and flow modelling complexity, starting from an isolated rotor in hover, and concluding with the complete helicopter configuration in forward-flight.

The paper will focus on the results of the activities undertaken by the four partners for the purpose of validating the CFD solvers prediction capabilities about an isolated rotor in hovering flight, and isolated fuselages in forward flight.

Nomenclature

c	- blade chord [m]
$C_d S$	- equivalent flat plate drag area [m] $= D/(1/2\rho v^2)$
c_{ref}	- blade chord of reference [m]
C_L	- average lift coefficient $= 6 \cdot T/(\rho\pi R^2 \sigma(\omega R)^2)$
C_P	- total power coefficient $= 8 \cdot Q/(\rho\pi R^2 \sigma(\omega R)^3)$
D	- fuselage drag [N]
FM	- Figure of Merit $= C_T\sqrt{C_T/2}/C_Q$
$M_{\omega R}$	- rotational tip Mach number
M_∞	- free stream Mach number
Q	- rotor torque, total power [N-m]
R	- rotor radius [m]
Re	- Reynolds number $= \rho v l/\mu$
T	- rotor thrust [N]
$y^+ = \rho_{wall} u_t y/\mu_{wall}$	being u_t the local tangential velocity and y the vertical direction

Greek letters

β_0	- coning angle at the blade root [degree]
υ	- cinematic viscosity $= \mu/\rho$
μ	- dynamic viscosity
ρ	- air density
σ	- rotor solidity $= cn/\pi R$
θ_0	- pitch angle at the blade root [degree]
θ_{07}	- pitch angle at 70% of radius [degree]
ω	- module of the rotational of the velocity field $= \nabla \times \mathbf{v}/a_\infty$

Acronyms

ATR	Advanced Technology Rotor
CFD	Computational Fluid Dynamics
CHANCE	Complete Helicopter AdvaNced Computational Environment
SGW2	Stoss/Grenzschicht Wechselwirkung 2

Subscripts

0	- mean or nominal value
∞	- free stream value

1 Introduction

The flow around realistic rotor blades is characterised by unsteady, non-linear, three-dimensional and transonic effects. In forward flight, on the advancing side of the rotor blade, transonic phenomena might occur, whereas dynamic stall conditions might be encountered on the retreating side. Furthermore, in both hover and forward-flight conditions, the blades shed complex vortical wakes which strongly influence the operating characteristics of the rotor. Helicopter fuselage shapes present particularly complex surfaces which deviate the flow and strongly modify its structure, thus generating early transition and many local separations with their inherent vortex shedding. Moreover, the mutual interactions between rotors and fuselage have strong influence on helicopter performance and handling qualities. In order to predict these complex flow phenomena accurately, numerical methods based on the solution of the Navier-Stokes equations with a sufficiently detailed grid, time interval and turbulence model have to be applied. Furthermore both multiblock and Chimera overlapping mesh techniques need to be mastered in parallel, to allow robustness and quality of the numerical solution, while minimising preparation and CPU time for an industrial application.

In research centres and universities, both in the US and Europe, considerable effort is being put into the development and validation of advanced CFD methods based on the solution of the Navier-Stokes equations. Within the frame of the French-German project CHANCE, the research institutes ONERA and DLR are enhancing the CFD flow solvers FLOWer and elsA, together with the helicopter manufacturer Eurocopter that is validating them against test cases of industrial interest. These CFD codes are also being integrated in rotor and fuselage design systems at Eurocopter [1]. The validation activity of the flow solvers will be achieved through intermediate stages of increasing geometry and flow modelling complexity, starting from an isolated rotor in hover and concluding with the complete helicopter configuration in forward-flight. The paper will focus on the results of the activities undertaken by the four partners for the purpose of validating the CFD solvers prediction capabilities about isolated rotors in hovering flight, and isolated fuselages in forward flight.

2 The Navier-Stokes flow solvers

2.1 The FLOWer code

The FLOWer flow solver [2],[3] is the Euler/Navier-Stokes code developed by DLR, which is being enhanced within the frame of the CHANCE project. It solves the compressible, three-dimensional Reynolds-averaged Navier-Stokes equations on block structured meshes around bodies in arbitrary motion. FLOWer implements two different spatial discretisation schemes, based on finite volume formulation, where the flow variables are located either at the vertices or at the cell centres.

The baseline method employs a central space discretisation with artificial viscosity and an explicit five stage Runge-Kutta time integration scheme. For steady computations, as it is the case in this paper, local time-stepping, implicit residual smoothing and multigrid can be used to accelerate convergence. Turbulence is modelled by algebraic or by more general transport equation models, *e.g.* two equation $k-\omega$ model. Low velocity preconditioning, deforming meshes and the Chimera technique are also available.

2.2 The elsA software

The elsA software is the new Object-Oriented multi-purpose CFD software for aerodynamics developed by ONERA, based on the solution of the Reynolds-Averaged Navier-Stokes equations. Its definition was started in 1997 and it combines the capabilities of the former ONERA CFD methods (CANARI, FLU3M, WAVES) which had various technical capabilities (such as multigrid, chimera, ALE), numerical schemes (centred, upwind schemes) or set of applications (subsonic / transonic, supersonic / hypersonic, rotating surfaces). The software combines C++ modules with encapsulated FORTRAN routines aiming at a better efficiency for scientific computing. Finally, the user interface is written in Python language, thus allowing higher-level communication for the elsA user. The method uses a cell-centred finite volume approach for multi-blocks structured grids. Although not all the previous functionality of CANARI, FLU3M and WAVES have yet been recovered, most of the applications previously completed with these methods can now be tackled with elsA. The developments made in elsA for helicopter applications have been presented in [4] and [5].

For helicopter applications, a second-order centred scheme with explicit artificial viscosity is coupled with a 4 stage Runge-Kutta time-stepping. Multigrid acceleration as well as local time-stepping and implicit residual smoothing are also used to reach the steady-state more efficiently. At present, for rotor applications turbulence is modelled with an algebraic Michel model, whereas a two transport equation k-l model is used for the fuselage.

3 Isolated rotor in hovering flight

Helicopters are the most efficient vehicles able to fly in hover condition, therefore hovering flight is definitely the most interesting flight condition of these machines. As opposed to forward flight, where the flow encountered by the rotor blades is unsteady, the flow in hover conditions is steady in a rotating frame of reference attached to the rotor blade. The complexity of the hovering flight is thus not related to unsteady phenomena or relative motion between the blades, as is the case for the forward flight, but to the complex vortical field shed by the blades during rotation. The vortices emitted by the rotor blades are the driving force for the downwash across the rotor disk and the wake contraction, which on their hand have a strong influence on the rotor loading and the induced power consumption. Therefore capturing these vortical phenomena is mandatory to compute accurately the rotor performance in hover (see also [6] and [7]).

This section presents the comparison between the numerical results of the FLOWer flow solver, about the Advanced Technology Rotor (ATR-A), and some flight test data available at Eurocopter Deutschland.

3.1 The Advanced Technology Rotor (ATR-A)

The ATR-A is the 4-bladed rotor mounted on the EC145 helicopter. Its blade (see Figure 1) features a tapered planform and a parabolic advanced tip shape. It uses the ONERA-Aerospatiale 4th series airfoils OA415, OA409 and OA407, and the 3rd series airfoil OA312. The maximum blade chord is of $c_{ref} = 0.362m$, and the rotor radius is of $R = 5.5m$.

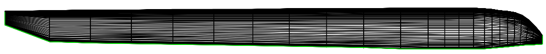

Figure 1: ATR-A blade grid (in each direction half of the points are shown for clarity)

Table 1 shows three flow field conditions which were selected from the flight test data base available at ECD with the purpose of validating the FLOWer code. The flight test data were recorded during the Donauwörth and Samedan EC145 flight campaigns. The helicopter weight, the total power measured at the engine drive shaft, the tail rotor power measured at the tail rotor drive shaft and all flight conditions are there stored. The main rotor thrust and power have then been post processed from the above mentioned data, by estimating the induced power, the gear box losses and the auxiliary power. These estimations might lead to an error of about 1% to 2% on the measured rotor thrust, and 3% to 4% on the estimated main rotor power consumption.

Case	$M_{\omega R}$	$Re\,[10^6]$
	[-]	[-]
1	0.668	6.15
2	0.652	5.27
3	0.645	4.55

Table 1: Flow field and rotor motion parameters, for the 3 considered test cases.

The trim conditions for all three cases of Table 1, *i.e.* the collective pitch θ_0 and the coning angle β_0 (see Table 2), plus the blade twist deformation, were computed by the CAMRAD II software. Two different inflow models were applied into CAMRAD for this purpose: the uniform inflow model and the prescribed wake inflow model. When the second inflow model is applied, the predicted elastic twist deformations at the blade tip are of about -1.0, -1.4 and -1.5 degrees, respectively for the flow conditions 1, 2 and 3 of Table 1. When the more simple uniform inflow model is used, all elastic blade twist deformations predicted by CAMRAD decrease, in absolute value, of about 0.5 degrees. In principle the prescribed wake inflow model is supposed to be more accurate than the uniform one, nevertheless this dependence of the FLOWer results from the CAMRAD II elastic torsion model has to be kept in mind.

Case	**Uniform Inflow**		**Prescribed wake Inflow**	
	θ_0	β_0	θ_0	β_0
1	13.0	2.5	12.9	2.6
2	15.2	3.4	15.4	3.4
3	16.6	3.5	16.8	3.5

Table 2: Collective pitch at the blade root and coning angles as computed by CAMRAD II for the 3 test cases.

The computational domains have been discretised using periodic C-H Navier-Stokes grids characterised by radial and vertical dimensions - both above and below the rotor - of 30 chords (1.97 R). The grids - one for each selected case - have been generated applying sequentially three different tools. Initially an Euler single block C-H periodic grid has been generated using the GEROS Euler grid generator [9]. Then the grid quality has been enhanced, as regards mesh orthogonality near solid surfaces, by using the smoother of the MEGACADS software [10]. Finally a number of boundary layer coordinate surfaces have been splined in. A tool developed by DLR, which modifies an Euler grid to generate a Navier-Stokes one by substituting the coordinate planes adjacent to a physical boundary, was used for this purpose.

Table 3 shows the grid dimensions used for the Euler and the Navier-Stokes grids. NI, NJ, NK are the volume grid dimensions (cells), respectively in chordwise, vertical and spanwise directions, whereas NI_{surf} and NK_{surf} are the surface grid dimensions (surface elements), respectively in the chordwise and spanwise directions.

Grid Type	**Dimensions**	**Surface grid dimensions**	**No. of nodes**
	NI x NJ x NK	NI_{sur} x Nk_{sur}	
Euler	208 x 32 x 72	160 x 48	503481
NS	208 x 48 x 72	160 x 48	747593

Table 3: Grid dimensions (cells)

Specifically for the ATR-A grid generation, starting from the C-H Euler grid, a Navier-Stokes one was generated by substituting the **5** J-planes adjacent to the blade surface with **21** J-coordinate planes, much closer to the blade surface. The minimum distance of the first plane is given to the spliner through input. Several NS grids can be generated starting from the Euler grid, depending on these input parameters. For our analysis the minimum distance of the first J coordinate plane from the blade surface was of 0.2E-5 chords. The calculated y^+ values (see Figure 3) are included in the range between 0.4 and 1.6 (the optimal range would be between 0 and 1), therefore the grid were considered fine enough to capture the strong gradients of the boundary layer. The y^+ values are relative to case 1, 2 and 3 for the elastic blade computation in the fully turbulent mode. Very similar values for the y^+ are found for the other FLOWer computations. The characterising properties of the grids (*e.g.* orthogonality, skewness, number of nodes, dimensions) used for this validation activity are the same. The grids differ only in the blade surface position. In fact for periodic grids the outer boundary must be kept fixed, thus each trim condition specifies a new position for the rotor blade. This means a new position of the inner grid boundary: blade surface, wake and tip slits. Figure 2 shows the Navier-Stokes grid used for the computation relative to the case 3 trim condition with the prescribed elastic twist applied.

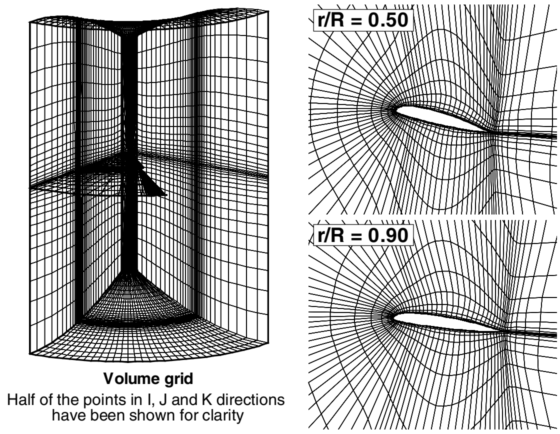

Figure 2: Navier-Stokes periodic single block C-H grid about the ATR-A blade.

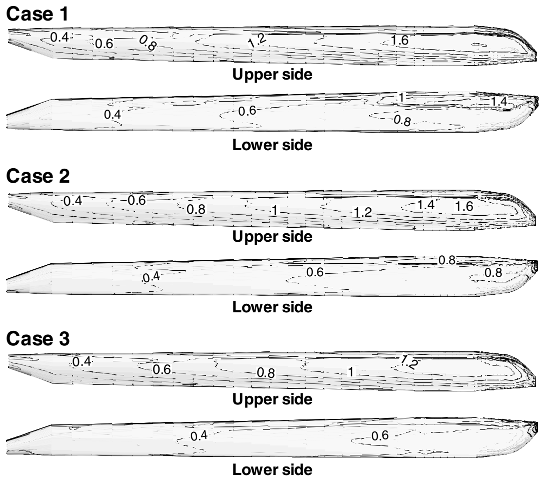

Figure 3: y^+ contour plots for case 1, 2 and 3 (elastic blade, fully turbulent computation)

All FLOWer computations (see Table 1) were run using the space central scheme with artificial dissipation according to Jameson, coupled with the 5-stage Runge-Kutta time discretisation scheme. The convergence has been accelerated by using local time stepping, implicit residual smoothing and 3 levels of multigrid. Two turbulence models, the algebraic Baldwin-Lomax and the two equation $k-\omega$ one, have been used. In the paper only the results relative to the more sophisticated $k-\omega$ turbulence model are shown. Each case has been run in three different modes, each of them characterised by the rigid/deforming blade assumption and by the laminar-turbulent transition line displacement. In the **first mode** the blade is rigid, *i.e.* no elastic twist has been applied, and the flow is fully turbulent, *i.e.* the transition from laminar to turbulent flow occurs at the blade leading edge. In the **second mode** the flow is always fully turbulent, but the blade is now elastic. Finally in the

third mode both elastic twist and laminar-turbulent transition are applied. In the current version of FLOWer no prediction of the laminar-turbulent transition is available, therefore the transition line had to be determined using another tool, specifically the 2D code SGW2 [10] of ECD. Then this information was given to FLOWer through input. The 2D flow around a number of blade sections taken along the blade span, from root to tip, was solved in order to determine the transition point on the upper and on the lower side of each section.

Figure 4 shows the convergence behaviour of the FLOWer code for the three test cases of Table 1 characterised by an elastically deformed rotor blade and a laminar-turbulent transition assigned. The convergence histories of the other two modes (*e.g.* fully turbulent flow about a rigid and an elastic rotor blade) are very similar. The residual plot shows the 3-step multigrid cycle composed by 500 iterations on the coarse grid level, 2000 on the medium and 2000 on the fine one. The convergence behaviour on the fine level shows a decrease of about four orders of magnitude.

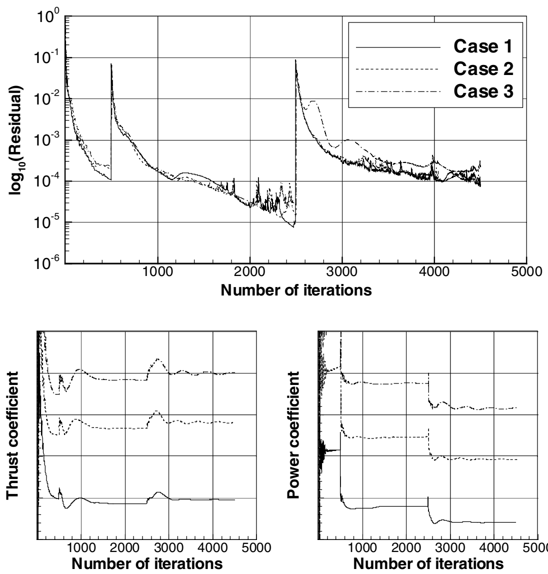

Figure 4: Convergence plots for case 1, 2 and 3 relative to the elastic blade calculation with the laminar-turbulent transition assigned.

Figure 6 shows the comparison among the rotor polar (*i.e.* total power coefficient C_P versus average lift coefficient C_L) computed with the FLOWer code in the three modes, and the flight test curve. The two fully turbulent modes are in good agreement with the flight test data, whereas the laminar-turbulent mode under-predicts the total power with respect to the flight test data of about 10% in all three computed points. The two fully turbulent modes appear shifted along the same curve, showing that the effect of the elastic twist decreases the lift and the drag accordingly, so that the computed points move along the polar curve. On the contrary, when the laminar region is considered in the numerical computation, as expected, a decrease of the power consumption is encountered (see Figure 8), whereas the lift remains almost unchanged (see Figure 7).

Figure 6 shows the same comparison of Figure 5 in terms of the figure of merit FM. For these figures the numerical computations, with both elastic torsion and laminar region accounted for, show a too optimistic prediction of the figure of merit: 5 to 6 points.

Figure 7 and Figure 8 show the comparison between the numerical results and the flight test data in terms, respectively of average lift coefficient and the total power coefficient, function of the collective pitch angle measured at 70% of the blade radius. It must be said that small differences between the pitch angle recorded during the flight tests and the values computed by CAMRAD II for the FLOWer trim conditions might exist, therefore the experimental curve might be shifted of some fraction of degree.

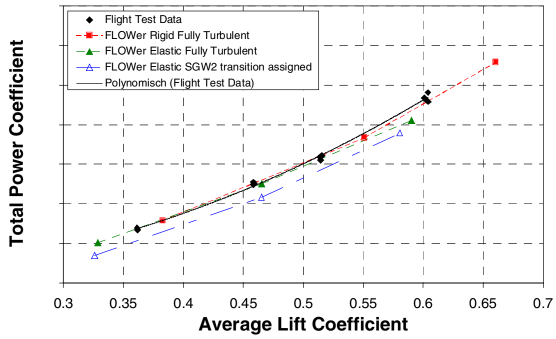

Figure 5: Rotor polar (drag coefficient as function of the lift coefficient). Comparison between numerical results and flight test data.

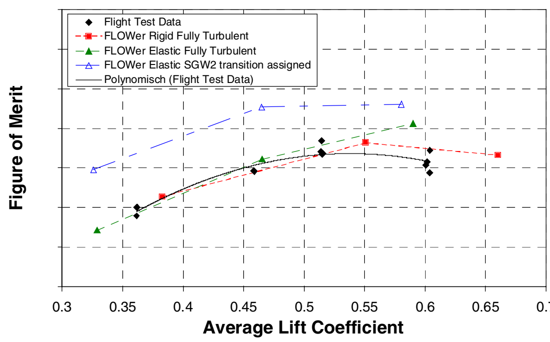

Figure 6: Figure of merit as function of the average lift coefficient. Comparison between numerical results and flight test data.

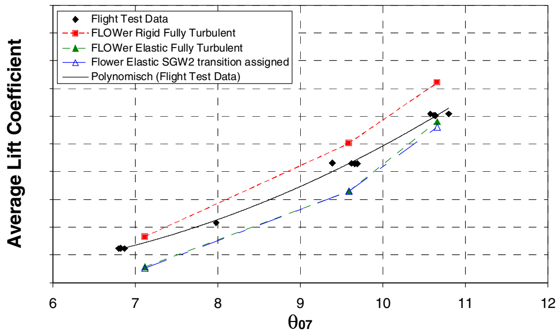

Figure 7: Average lift coefficient as function of the collective pitch angle in degree at 70% of the rotor blade radius. Comparison between numerical results and flight test data.

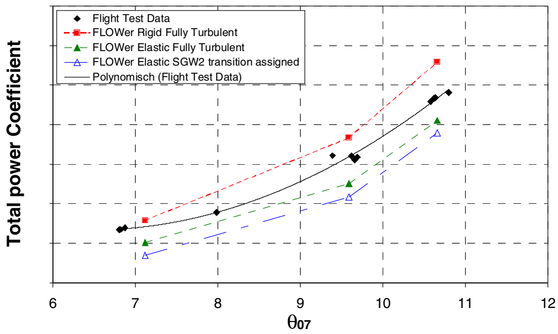

Figure 8: Average total power coefficient as function of the collective pitch angle in degree at 70% of the rotor blade radius. Comparison between numerical results and flight test data.

Figure 9 and Figure 10 show respectively the radial contraction and the vertical position of the blade tip vortex core, function of the vortex age, whereas Figure 11 shows the tip-vortex strength evolution function of the vortex age. These plots are relative to the FLOWer run in the third mode: elastic blade and laminar-turbulent transition assigned. The radial contractions are very similar for all three cases considered. The vertical evolution of the vortex is characterised by an increase of the vertical position in its first 90° of life, then the interaction with the following blade pushes the tip vortex further downstream. This shows that an orthogonal blade-vortex interaction is quite important and that differences in the thrust and power might be encountered if the tip vortex is less dissipated. In fact, as shown in Figure 11 the vortex dissipates quite rapidly during the first 60 degrees of its life, then its intensity keeps constant for other 60 degrees, till it decreases again. A local grid refinement in the tip-vortex region shall be envisaged to decrease the vortex dissipation.

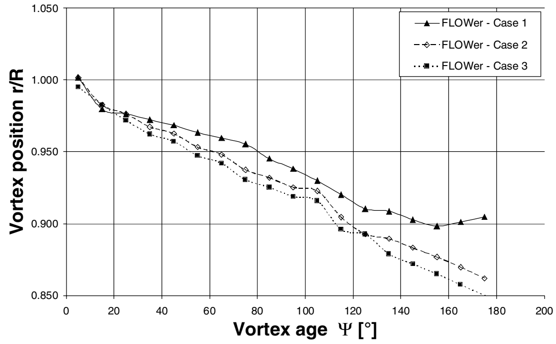

Figure 9: Radial contraction of the tip vortex. Comparison among the three FLOWer computations.
(Elastic blade and laminar-turbulent transition assigned)

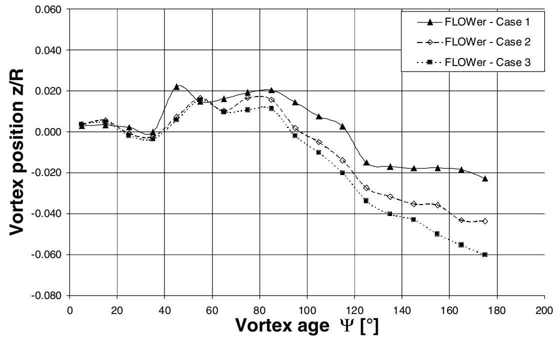

Figure 10: Vertical evolution of the tip vortex. Comparison among the three FLOWer computations.
(Elastic blade and laminar-turbulent transition assigned)

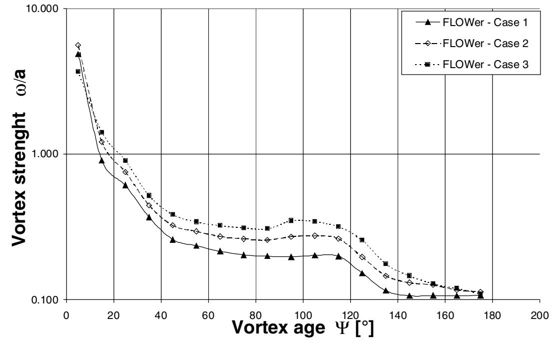

Figure 11: Tip vortex strength comparison for the three FLOWer computations.
(Elastic blade and laminar-turbulent transition assigned)

As discussed in [8], at low disk loading (*e.g.* case 1 and 2 of Table 1) a stronger tip vortex core shall induce higher velocities in the tip region, which would locally increase the angle of attack, thus decreasing the figure of merit (about 2 points), because of worst thrust over power ratios. For higher disk loading (*e.g.* case 3 of Table 1) such considerations are not straightforward due to flow separation which might occur at the blade trailing edge towards the blade root.

In conclusion, even though the fully turbulent computations seem more reliable, the small uncertainties due to post processing of the flight test data, the 2D approximation in the calculation of the laminar-turbulent transition line, and the important numerical tip vortex wake diffusion in the CFD calculations, might change the comparisons in favour of the laminar-turbulent FLOWer numerical results. Further computations on refined meshes in the tip vortex region are foreseen.

4 Isolated fuselage in forward flight

Nowadays the aerodynamic department of helicopter manufacturers uses CFD for the flow field analysis of fuselage as well as of isolated rotors. CFD is currently in use at Eurocopter for several applications such as:

- supplement the wind tunnel tests and provide surface pressure distribution as input for stress analysis of fuselage structure components *i.e.* doors, horizontal stabilisers, endplates etc. [9];
- optimise the aerodynamic design of fuselages and fuselages parts *i.e.* air inlet geometry, engine outlet etc.

This section presents two validation cases for the elsA flow solver. The first test case deals with the Dauphin HELIFUSE geometry, whereas the second regards the NH90 fuselage.

4.1 The Dauphin test case

The Dauphin case is one of the HELIFUSE test cases [13], for which extensive and well-documented experimental data, as well as various Navier-Stokes flow solutions exist, coming from the various Partners of the HELIFUSE project. This makes of the Dauphin case a perfect portability test, *i.e.* for each new software release, thus for each new installation on the industrial site, this test case is run.

This is a high-speed, high-Reynolds number case (M_∞=0.235, Re=30 Million). Finally, the angles of incidence and of side slip are set to 0°. For the present case, the grid was generated by ONERA using the ICEM-CFD MULCADS grid generator, which was the standard ICEM grid generation tool for structured grids before HEXA. This grid is made of 10 blocks and includes 1,207,650 points. Its structure allows the use of 3-level multigrid techniques. In the present case, a w-cycle multigrid was used, since it proved the most efficient in convergence acceleration for such kind of configuration. The elsA computation was made assuming a fully turbulent flow, using the 2-equation k-l turbulence model. The grid is fine enough in order to have a proper discretisation of the boundary layer, with a maximum y^+ at the fuselage surface of less than 0.5 (see Figure 12).

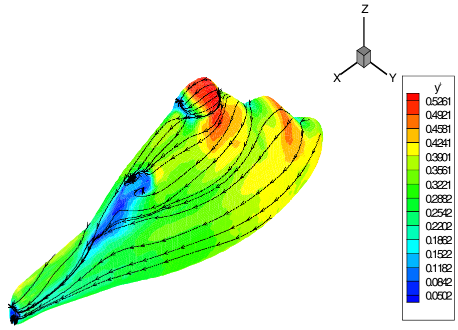

Figure 12: y^+ contour plot on the fuselage surface

The flow solution is very close to that obtained with CANARI or other RANS methods, and in reasonable agreement with experiment as shown by Figure 13. It shows the pressure distribution along the fuselage centreline. Indeed, the major discrepancy between computations and experiment appears on the bottom centreline. In fact, in that region the wind tunnel model is attached to the strut, which locally modifies the flow field.

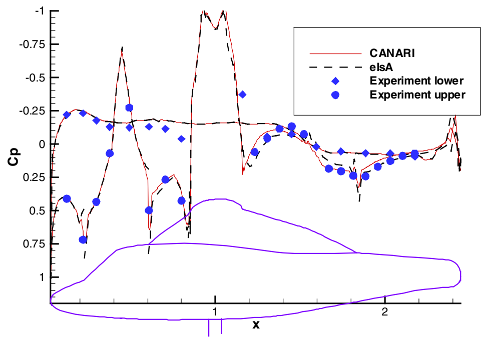

Figure 13: Pressure distribution on the DGV fuselage

4.2 The NH90 test case

The NH90 helicopter has been chosen as a validation test case of industrial interest for the CFD elsA software due to its complex but realistic shape. The rear part, the sponson, the engine fairing and IRS fairing have been taken into account for the Navier-Stokes calculation. The CAD shape has been cleaned and simplified by means of the CATIA tool (Figure 14) and the grid has been created with the ICEM-HEXA grid generator (Figure 15). The resulting mesh is composed of 4.5 million nodes and allows a 2 level multigrid for the acceleration of convergence. The calculated y^+ have a mean value of 0.5, therefore the grid has been considered as fine enough to capture the strong gradients in the boundary layer. The mesh is adapted for a 6 processors calculation with 6 Go of memory in order to have a calculation feedback time of 2 days on a SGI3400 computer.

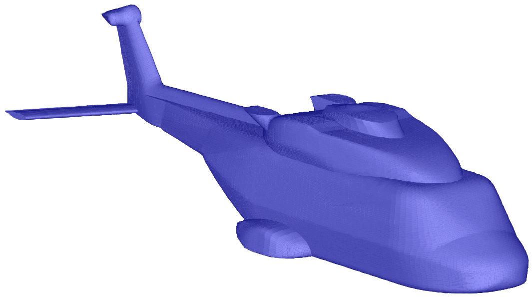

Figure 14: Shape of the NH90 fuselage

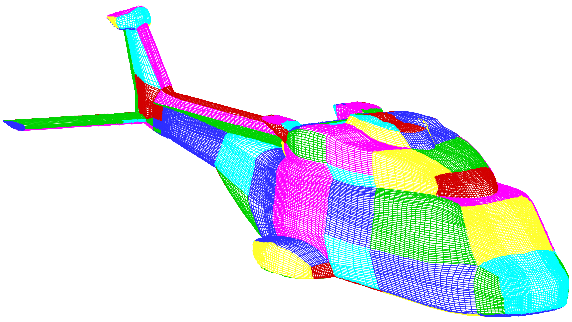

Figure 15: Grid of the NH90 fuselage
(4.5 millions points)

The test case configurations have been selected from the LST campaign test matrix (Low Speed Tunnel at DNW) for the 1/10 model scale. The pitch attitude are 0° and –4° for a flight velocity of 40m/s. The calculation process is initialised by 20 laminar cycles, and then the turbulent viscosity is set to 10 times the kinematic viscosity to start the fully turbulent computation, using the k-l model of Smith. 2000 cycles have been performed in order to achieve convergence on both residuals and integrated performance (drag coefficient) (Figure 16).

The pressure field obtained (Figure 17) is in good agreement with the flow physics and some comparison made with experiment on sensitive areas like the aft body, where separation occurs, is fairly satisfactory (Figure 18).

Indeed, the experimental pressure coefficient distribution of Figure 18 show separation in the x range between 11000 and 12000, where the pressure coefficient is zero. The numerical prediction detects local separation at $x = 11000$, after a strong recompression, but the flows reattaches earlier. Mesh refinement in this sensitive area could eventually improve the calculation.

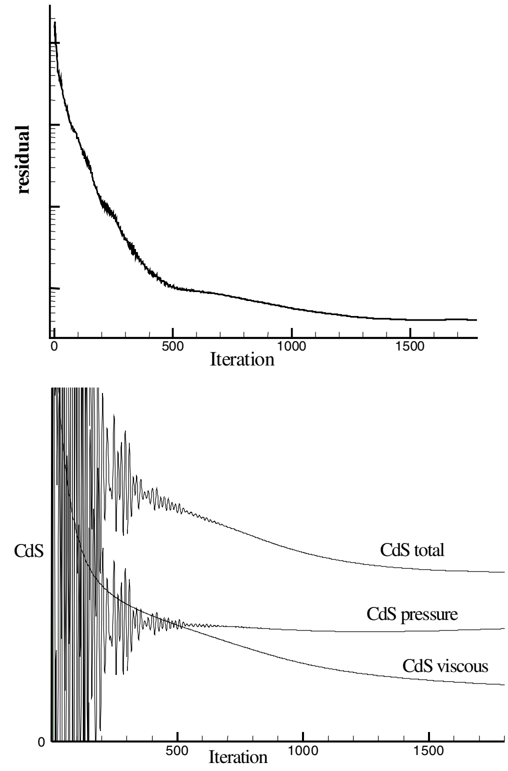

Figure 16: Residuals and C_dS convergence

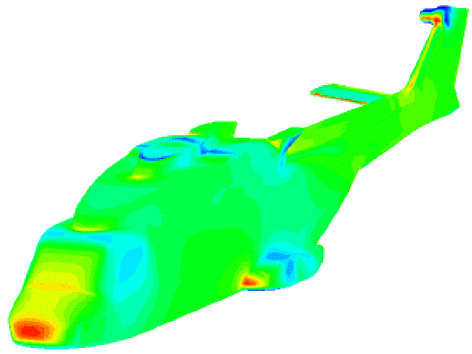

Figure 17: View of the pressure coefficient on the NH90 fuselage (40m/s, 0°, 1/10 scale)

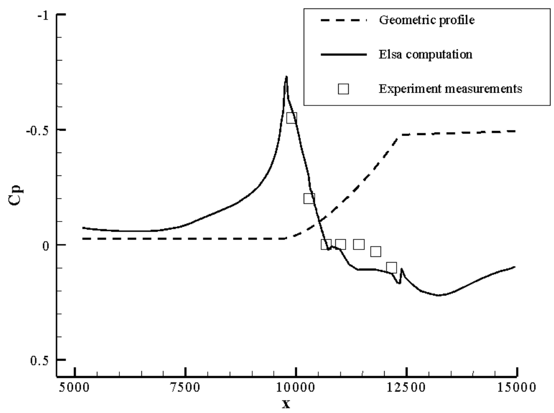

Figure 18: Comparison of pressure coefficient on the centre line of the aft body (40m/s, 0°, 1/10 scale) with LST experiment.

For aerodynamic performance prediction the C_dS value between LST wind tunnel and elsA calculation were compared. The reference area is chosen to be equal to the full scale area for all calculation as well as for measurement. As it could be expected, the elsA calculation overestimates the C_dS value. Indeed, the fully turbulent Navier-Stokes model could be responsible of around 50 % of error on the viscous terms contribution for model scale leading to an average 20% error on the total drag. Another source of discrepancies lies in the influence of the strut in the experiment and thus in the correction used for comparison with isolated fuselage calculation. The strut leads currently to an increase of around 10% to 20% on the measured drag coefficient, as shown in [13], that has to be corrected usually by the drag of the strut alone (Table 4).

Experiment (with strut effect)	Experiment (corrected with strut effect)	Elsa calculation (Fully turbulent)	Elsa calculation (corrected of laminar viscosity)
+15%	reference	+55%	+35%

Table 4: Elsa calculation and LST experiment comparison

Another source of error is probably due to the pressure terms contribution. The 4.5 millions points grid exhibits weak refinement near some of the stagnation points or in the separation area. We know that the drag prediction is very sensitive to the mesh in this area, since the orientation of the surface makes the drag value very sensitive to the pressure values in this region. Therefore, for these complex fuselage shapes, 4.5 millions points seems to be the minimum size required and the use of finer grid should reduce the discrepancies compared with experiment.

For industrial purposes, we are interested in the C_dS variation with parameters like pitch attitude for helicopter performance and trim, Reynolds number for scale influence or shape variation for optimised design. The corresponding calculation at full scale and at 1/3 model scale have then been performed for the two pitch attitudes. On Figure 19, it is shown that the calculated C_dS versus pitch attitude is very close to the experimental one. An increase of 11% from 0° to –4° for both, experiment and calculation can be observed.

The experimental variation of Reynolds is obtained by increasing the free stream velocity from 40m/s to 75m/s. In the calculation the Reynolds variation is obtained by changing the scale. The experimental and the calculated variations are similar (Figure 20): in the two cases, a decrease of the drag coefficient of the same amplitude can be noticed.

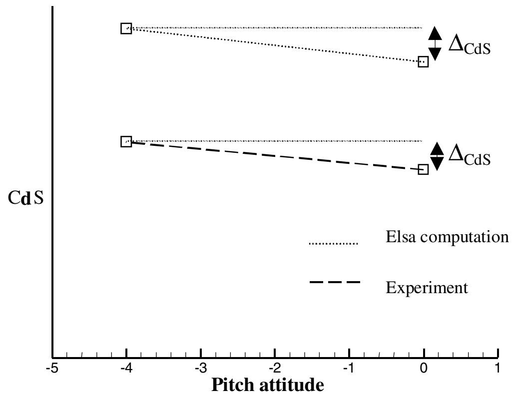

Figure 19: Variation of C_dS versus pitch attitude (40m/s, 1/10 scale)

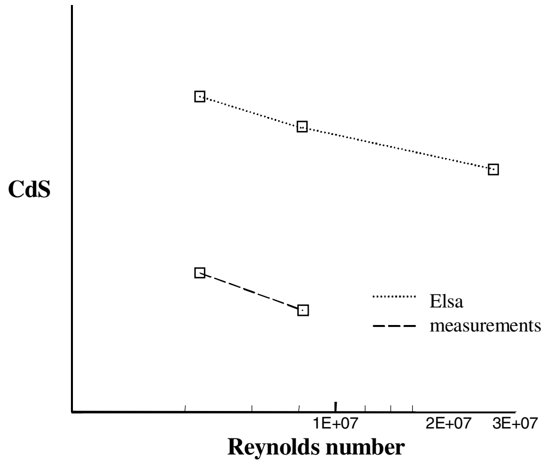

Figure 20: Variation of C_dS versus Reynolds number (0° of pitch attitude)

5 Conclusions

The FLOWer and elsA CFD flow solvers, under development respectively at DLR and ONERA within the joined French-German project CHANCE, are being validated on cases of industrial interest by Eurocopter. The paper has presented the validation of the FLOWer code about the ATR-A rotor of the EC145 helicopter in hovering conditions, and of the elsA software about the Dauphin and NH90 helicopter fuselages in forward flight conditions. Both codes showed a good and robust convergence and in all cases the numerical predictions have showed a satisfactory agreement with the experimental data, *e.g.* wind tunnel or flight test data. The future validation activities of the FLOWer and elsA codes will focus on isolated rotor in forward flight and helicopter fuselage, with an actuator disk model simulating the main rotor induced flow, in forward flight conditions.

In conclusion, thanks to the large progress in CFD tools (numerical model, convergence techniques, parallel computation, etc) and in computer performance, it is nowadays possible to predict a lot of complex aerodynamic phenomena with enough accuracy and within an acceptable feedback calculation time, *i.e.* less than 3 days in industrial environment. CFD tools will help investigating some very complex phenomena usually difficult or expensive to analyse with wind tunnel facilities alone. They seem to be mature enough to drive optimisation design and thus dramatically reduce development costs, although wind tunnel tests still remain the ultimate judge in confidence.

6 Acknoledgments

The authors would like to thank the French DPAC and German BMWi for their support.

References

[1] G. Arnaud, A. D'Alascio, C. Castellin, L. Sudre, J.-M. Rodriguez, "*The Helicostation – A necessary computing environment for CFD applications in industry",* Proceedings of the 27th European Rotorcraft Forum, Moscow, Russia, September 2001.

[2] N. Kroll, C.-C. Rossow, K. Becker and F. Thiele *"The MEGAFLOW Project" Aerospace Sciences Technology Vol. 4 (2000),* pages 223-237.

[3] N. Kroll, B. Eisfeld, and H.M. Bleecke. "*The Navier-Stokes Code FLOWer", volume 71 of Notes on Numerical Fluid Mechanics,* pages 58-71. Vieweg, Braunschweig, 1999.

[4] J.-C Boniface, B. Cantaloube and A. Jolles, "*Rotorcraft Simulation Using an Object Oriented Approach",* Proceedings of the 26th European Rotorcraft Forum, The Hague, The Netherlands , September 2000.

[5] C. Benoit and G. Jeanfaivre, "*3D Inviscid Isolated Rotor and Fuselage Calculation Using Chimera and Automatic Cartesian Partitioning Methods",* AHS, Aeromechanics 2000, Atlanta (USA), November 2000.

[6] P. Beaumier, E. Chelli and K. Pahlke, "*Navier Stokes Prediction of Helicopter Rotor Performance in Hover including Aero-elastic Effects",* Presented at the American Helicopter Society 56th Annual Forum, Virginia Beach, Virginia, May 2000.

[7] J. U. Ahmad and R. C. Strawn, "Hovering rotor and Wake Calculation with an Overset-Grid *Navier Stokes Solver",* Presented at the American Helicopter Society 55th Annual Forum, Montreal, Canada, May 1999.

[8] P. Beumier, C. Castellin and G. Arnaud, "Performance Prediction and Flow Field Analysis of Rotors in Hover, Using a Coupled Euler/Boundary Layer method*",* Proceedings of the 24th European Rotorcraft Forum, Marseille, France, September 1998.

[9] P. Renzoni, A. D'Alascio, N. Kroll, D. Peshkin, M. H.L. Hounjet, J-C. Boniface, L. Vigevano, L. Morino, C. B. Allen, K. Badcock, L. Mottura, E. Schöll and A. Kokkalis, "*A common European Euler code for the analysis of the helicopter rotor flowfield",* Progress in Aerospace Sciences, Vol. 36, 2000, pp 437-485.

[10] O. Brodersen, M. Hepperle, A. Ronzheimer, C.-C. Rossow and B. Schoenig *"The parametric Grid Generation System MegaCads",* Proceedings of the 5th International Conference on Numerical Grid Generation in Computational Field Simulations, Ed: B.K. Sony, J.F. Thompson, J. Haeuser, P. Eisemann, NSF Mississippi, pp.353-362, 1996.

[11] G. Dargel and P. Thiede, *"Viscous Transonic Airfoil Flow Simulation by an efficient Viscous-Inviscid interaction Method",* **AIAA-87-0412**, Messerschmitt-Bolkow-Blohm GmbH, Bremen, FRG.

[12] E. Schöll, "Numerical simulation of the BK117 / EC145 Fusealge Flow Field.*",* Proceedings of the 25th European Rotorcraft Forum, Rome, Italy, September 1999.

[13] V. Gleize, M. Costes, H.Frhr. von Geyr, N. Kroll, P. Renzoni, M. Amato, A. Kokkalis, L. Mottura, C. Serr, E. Larrey, A Filippone and A. Fischer *"Helicopter Fuselage Drag Prediction: State of the Art in Europe",* **AIAA** Paper No. **2001-0999**, 39th AIAA Aerospace Sciences Meeting & Exhibit, Reno NV, January 2001.